small
NANO MICRO
www.small-journal.com

Palladium-Decorated Silicon Nanomesh Fabricated by Nanosphere Lithography for High Performance, Room Temperature Hydrogen Sensing

*Min Gao, Minkyu Cho, Hyeuk-Jin Han, Yeon Sik Jung, and Inkyu Park**

A hydrogen (H_2) gas sensor based on a silicon (Si) nanomesh structure decorated with palladium (Pd) nanoparticles is fabricated via polystyrene nanosphere lithography and top-down fabrication processes. The gas sensor shows dramatically improved H_2 gas sensitivity compared with an Si thin film sensor without nanopatterns. Furthermore, a buffered oxide etchant treatment of the Si nanomesh structure results in an additional performance improvement. The final sensor device shows fast H_2 response and high selectivity to H_2 gas among other gases. The sensing performance is stable and shows repeatable responses in both dry and high humidity ambient environments. The sensor also shows high stability without noticeable performance degradation after one month. This approach allows the facile fabrication of high performance H_2 sensors via a cost-effective, complementary metal–oxide–semiconductor (CMOS) compatible, and scalable nanopatterning method.

1. Introduction

Hydrogen (H_2) is widely considered to be one of the most promising next-generation energy resources, mainly because it can be practically acquired in large amounts, and no hazardous byproducts are created during the energy generation process.[1,2] H_2 is also a very important material for various industrial applications, including hydrogen-cooled systems, petroleum refinement, and metallurgic processes, because of its reactive chemical properties and unique physical properties.[3–5] However, H_2 is an explosive gas with a lower flammable limit (LFL) of 4% in air.[6] Moreover, H_2 is colorless and odorless, which makes it difficult to detect with human senses.[7] Therefore, developing H_2 gas sensors with high sensitivity, fast response, high selectivity, and good stability, is of significant importance for the rising H_2 economy.

Palladium (Pd) has been extensively used as a functional material for H_2 detection, since it can easily absorb H_2 gas and converts to palladium hydride (PdH_x) at room temperature, which changes the material's electrical properties.[8] This change in electrical properties in the presence of H_2 allows Pd or Pd hybrid materials to be utilized as H_2 sensors.[9–12] Among all such materials, Pd-Si-based devices have attracted considerable attention because of their compatibility with conventional complementary metal–oxide–semiconductor (CMOS) process technology.[3,11] The sensing mechanism in Pd-gated Si devices has been well developed. When exposed to H_2 gas, H atoms dissociated from the H_2 molecules are dissolved into the Pd metal, which becomes polarized in the vicinity of the boundary with an underlying insulation layer, and this modulates the electrical carrier concentration in the semiconductor layer underneath.[13] Unlike the metal oxide or other semiconductor materials, Si itself is inert to most gas components. Also, Si can be easily decorated with various materials to create sensitivity to particular target gases. This enables the functionalized Si device to have excellent selectivity against introduced chemical or biological species.[14–16]

Si nanowire-based devices have been employed as efficient components in high performance sensors for detecting gases and other chemical and biological components.[17–21] Since the nanowires have a high surface-to-volume ratio, they respond more sensitively to the surrounding environment.

The techniques used to fabricate Si nanowires can be categorized into bottom-up[22–24] or top-down[25–27] approaches. The bottom-up fabrication routine can produce high yields of nanoscale structures at low cost. However, it suffers from poor reproducibility and difficult device integration.[28,29] The standard top-down routine requires high-resolution lithography techniques such as electron beam (E-beam) lithography[26,27] to achieve nanoscale patterns. Although nanostructures with dimensions down to a few nanometers can be achieved using the top-down techniques, their high cost and low yields make them impractical for low-cost mass production.[30,31]

The nanosphere lithography (NSL) method, also known as colloidal lithography or natural lithography,[32,33] utilizes the self-assembly of a nanosphere monolayer and could be an alternative choice for achieving uniform and well-ordered nanopatterns with minimum sub-10 nm dimensions.[34,35] At the same time, the NSL method is scalable up to wafer-level fabrication with high yield and is compatible with the conventional CMOS process.[36] Various nanostructures and applications based on this method have been reported.[37–39] For example, well-ordered and high-aspect-ratio Si nanowires have been fabricated using

M. Gao, Dr. M. Cho, Prof. I. Park
Department of Mechanical Engineering
Korea Advanced Institute of Technology
Daejeon 34141, Korea
E-mail: inkyu@kaist.ac.kr
H.-J. Han, Prof. Y. S. Jung
Department of Material Science and Engineering
Korea Advanced Institute of Technology
Daejeon 34141, Korea

DOI: 10.1002/smll.201703691

a combination of NSL and metal-assisted etching of Si, and those structures have already shown remarkable performance in sensor related applications.[40,41]

In the present paper, we present a novel H_2 sensor based on a Pd-decorated Si nanomesh structure patterned using the polystyrene nanosphere lithography (PS-NSL) method. In this method, an oxygen (O_2) plasma treated polystyrene (PS) monolayer is employed as a reverse template for a Cr mask pattern with a feature size of 50–80 nm, which is then transferred to an Si nanopattern through single-step Si dry etching with SF_6/O_2 plasma. Following the Si nanomesh fabrication, the device is treated by buffered oxide etchant (BOE) solution to induce a rough surface[42,43] which provides more space for loading Pd nanoparticles (PdNPs), which improves the sensing performance. The PdNPs decoration gives the structure highly selective H_2 gas sensitivity.

2. Results and Discussion

The fabrication process for the Si nanomesh sensor device is explained in **Figure 1** and Figure S1 in the Supporting Information. A high-level arsenic (As) doping process was applied at the source and drain regions (n^+-Si) by ion implantation while the channel area was covered by photoresist as a doping mask, followed by a low-level phosphorus (P) doping process to the entire active area. In this way, an n^+–n^-–n^+ structure was formed as the framework of the sensor device (Figure 1a). A thin Cr protection layer (thickness: 10 nm) was deposited on top of the source and drain regions (Figure S1-ii, Supporting Information) by electron beam (e-beam) evaporation to protect the Si layer from being etched in the later PS-NSL process. A compact PS nanosphere (diameter: 500 nm) monolayer was formed on the substrate via a multistep spin

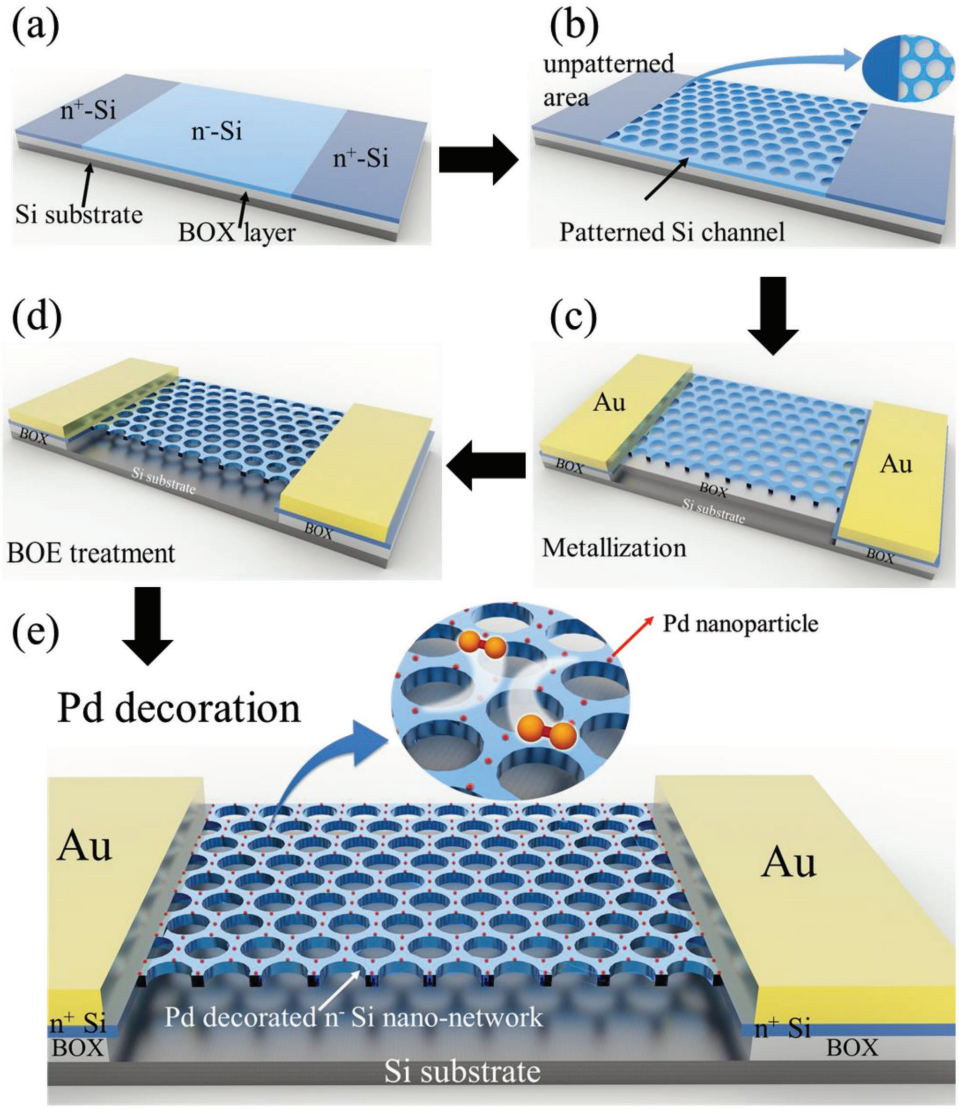

Figure 1. Schematic of the fabrication process for the Pd-decorated Si nanomesh H_2 sensor: a) ion implantation for n^+-Si and n^--Si areas, b) nanomesh pattern formation in the n^--Si channel via the PS-NSL process, c) contact electrode formation in the source and drain regions, d) BOE treatment to create a rough surface on the Si nanomesh structure, and e) surface functionalization of the Si channel with PdNPs via e-beam evaporation.

coating process (Figure S1-iii, Supporting Information).[44,45] The PS beads shrunk during exposure to the O_2 plasma using reactive-ion-etching (RIE) process, which generated nanometer-size gaps between individual beads (Figure S1-iv, Supporting Information). After another Cr layer was deposited, the PS beads were removed in a deionized (DI) water bath under mild sonication, and a Cr mask layer with nanomesh pattern was formed (Figure S1-v, Supporting Information). Afterward, the same pattern was transferred to the Si layer via RIE process using SF_6 and O_2. Since the source and drain areas were protected by the Cr protection layer deposited in advance (Figure S1-ii, Supporting Information), only the low-doped Si channel area was etched (Figure S1-vi, Supporting Information). After removing all Cr layers on top, a honeycomb-like Si nanomesh channel was formed (Figure 1b). The electrode contact was later defined via a conventional metal lift-off process (Figure 1c). Then, BOE treatment was used to clear the surface contamination as well as to modify the surface morphology of the Si structure,[42,43] enhancing the sensing performance.

Because the Si channel has a nanomesh geometry and thus contained many etching holes, the buried oxide (BOX) layer underneath the channel area was also removed during the BOE treatment process, and the channel became suspended from the substrate (Figure 1d). Finally, Pd was deposited on the Si channel by e-beam evaporation to achieve sensitivity and selectivity to H_2. Figure 1e schematically presents the sensor device with the BOE treated Si nanomesh structure. Since the preset deposition thickness is too small (1 nm) to form a continuous thin film, Pd is expected to aggregate as isolated particles on the Si oxide surface.[3] This is due to the high surface energy of the thin Pd layer and relatively low surface energy of the Si oxide.[46]

After the subsequent fabrication steps, the structures were observed by scanning electron microscopy (SEM) and atomic force microscopy (AFM) as shown in **Figure 2**. Figure 2a,b depicts the surface morphology of the compact PS nanosphere (average diameter: 500 nm) monolayer, and the pattern with gaps of ≈80 nm between individual beads after the O_2 plasma

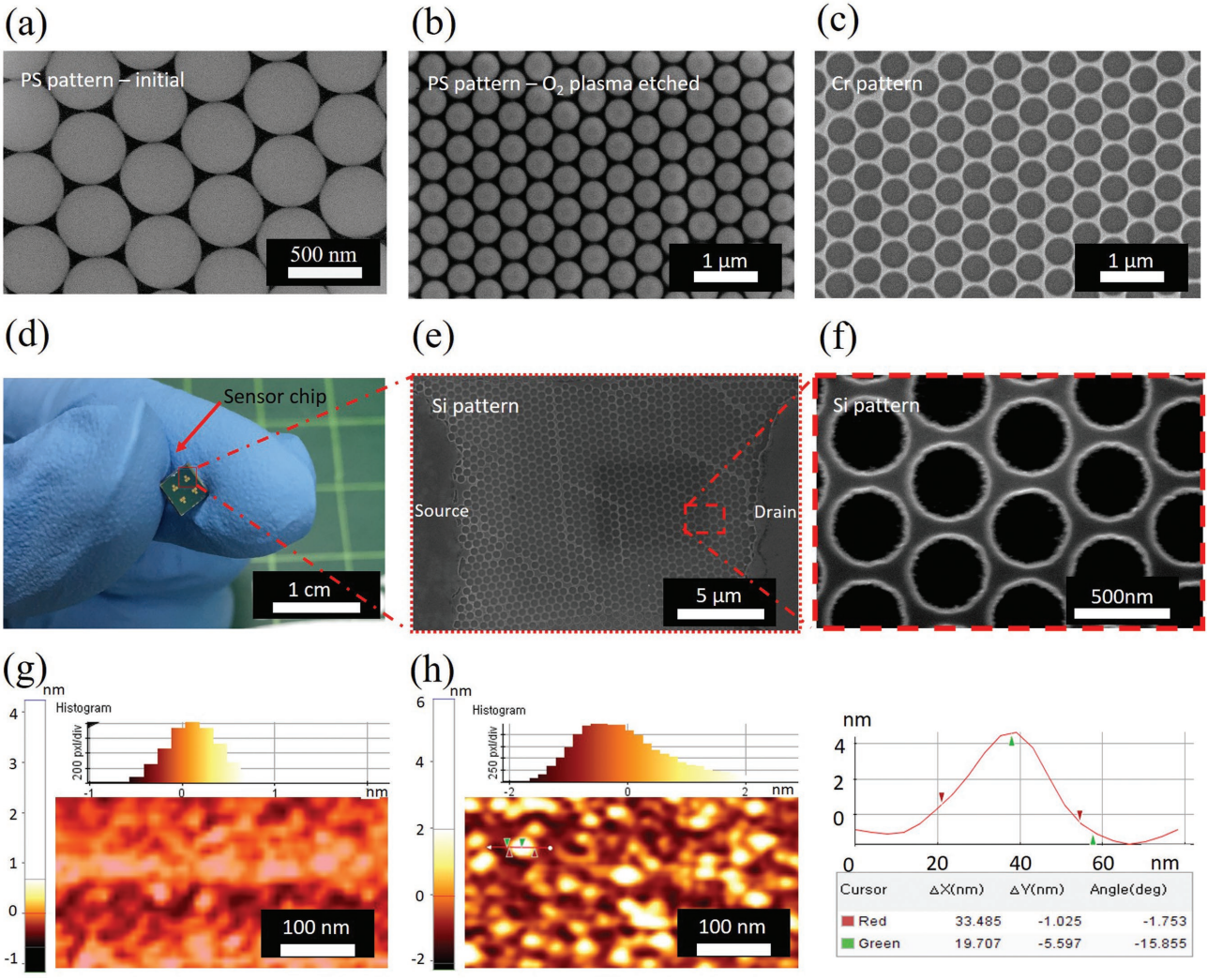

Figure 2. Characterization of device morphology: SEM images of a) PS compact monolayer pattern at the initial state (diameter: 500 nm), b) PS pattern after O_2 plasma etching for 25 s, c) Cr reverse-pattern produced by e-beam evaporation and PS lift-off, d) sensor device on a 4 × 4 mm^2 chip, e) top view of the whole channel area with Si nanomesh structure, f) close-up view of the Si nanomesh structure, g) AFM image for the Si surface without Pd decoration, and h) AFM image of the Si surface with Pd decoration and a surface profile of a single Pd nanoparticle deposited on the Si surface.

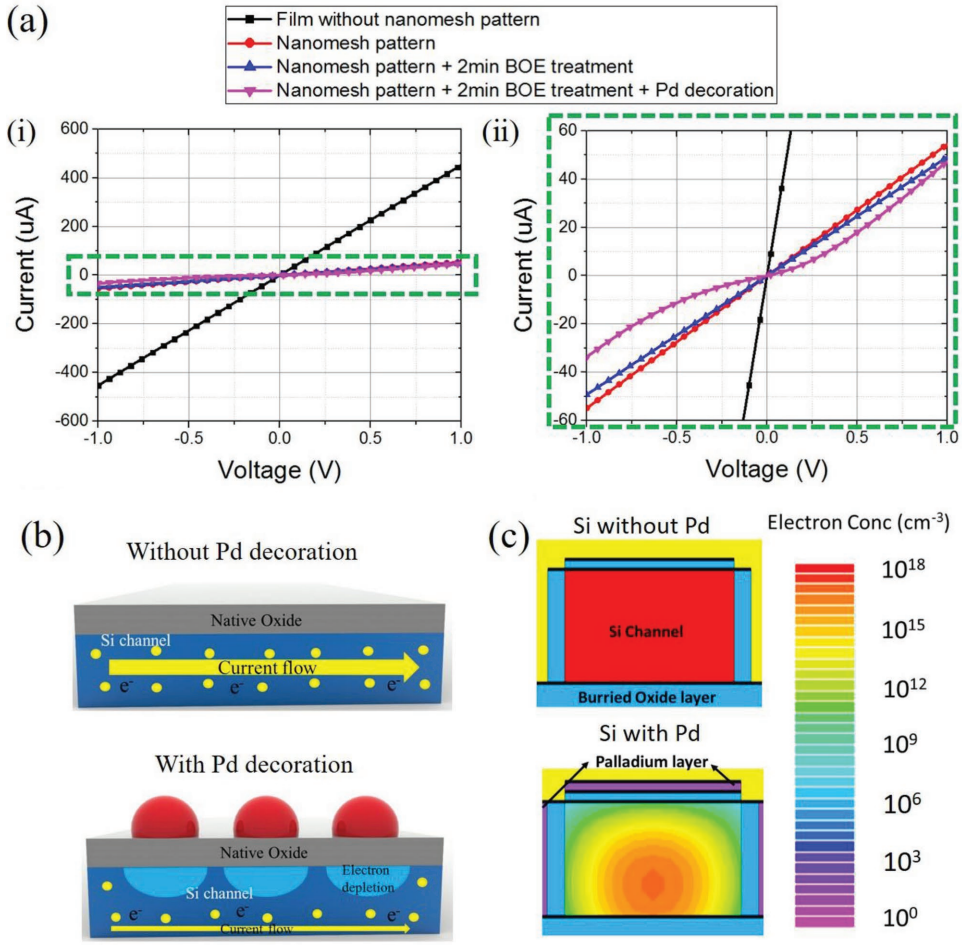

Figure 3. Electrical characterization of the fabricated device: a-i) *I–V* curves of the n^+–n^-–n^+ Si structure corresponding to the sequential fabrication processes (nanomesh patterning via the PS-NSL, BOE treatment for the Si channel, and Pd decoration on Si surface), with (a-ii) a close-up view in the dotted green box; b) schematics of the resistance change in the Si channel with and without Pd decoration; c) electron concentration before and after setting the Pd layer with a work function of 5.12 eV on the Si surface, by numerical simulation.

etching. The images of the compact PS monolayer pattern formed on the substrate, and the evolution of PS beads by O_2 plasma etching, are presented in Figure S2 in the Supporting Information. The Cr mask pattern was successfully created after the deposition of Cr by e-beam evaporation and lift-off of the PS beads (Figure 2c).

The fabrication process was applied to a 2 cm square chip which was later cut into a 4 mm square size (Figure 2d). Figure 2e shows the morphology of the entire Si nanomesh channel after the RIE and Cr removal steps, which confirms the uniformity of the patterned Si channel. A close-up view of the Si nanomesh pattern is presented in Figure 2f. The minimum width at the center of a single wire is 40–50 nm at the top and 70–80 nm at the bottom. These unequal widths are caused by the undercut during the SF_6/O_2 plasma etching process of Si. This wedge shape offers more loading space, allowing the Pd to be decorated on the sidewall, which is good for the sensing performance.

To investigate the BOE etching effect on the n^--Si channel, a flat silicon-on-insulator (SOI) chip with the same doping conditions was used for convenience of analysis. The surface morphologies before and after BOE treatment for 2 min are shown in Figure S3 in the Supporting Information. The root mean square (RMS) value of the surface roughness increased from 0.344 nm for the SOI substrate to 0.66 nm after the BOE treatment.

The surface morphology of the nonpatterned Si surface is illustrated in Figure 2g. Figure 2h shows the AFM image of the morphology of the PdNPs deposited on the Si surface by e-beam evaporation with 1 nm preset thickness (deposition rate: 0.2–0.3 Å s^{-1}), with the quantitative parameters shown in the bottom right corner. Here, the PdNPs have a thickness of 4–5 nm and diameters from several nanometers to 50 nm.

Figure 3 depicts the electrical characteristics of the n^+–n^-–n^+ Si structure after each fabrication step (nanomesh patterning via the PS-NSL, BOE treatment for the Si channel, and Pd decoration on Si surface). In Figure 3a, we can clearly observe there was an eight times increase in electrical resistance after the honeycomb-like nanomesh pattern was formed via the PS-NSL. The changes after the subsequent steps are shown on the right side of Figure 3a. A slight resistance increase is observed after 2 min of BOE

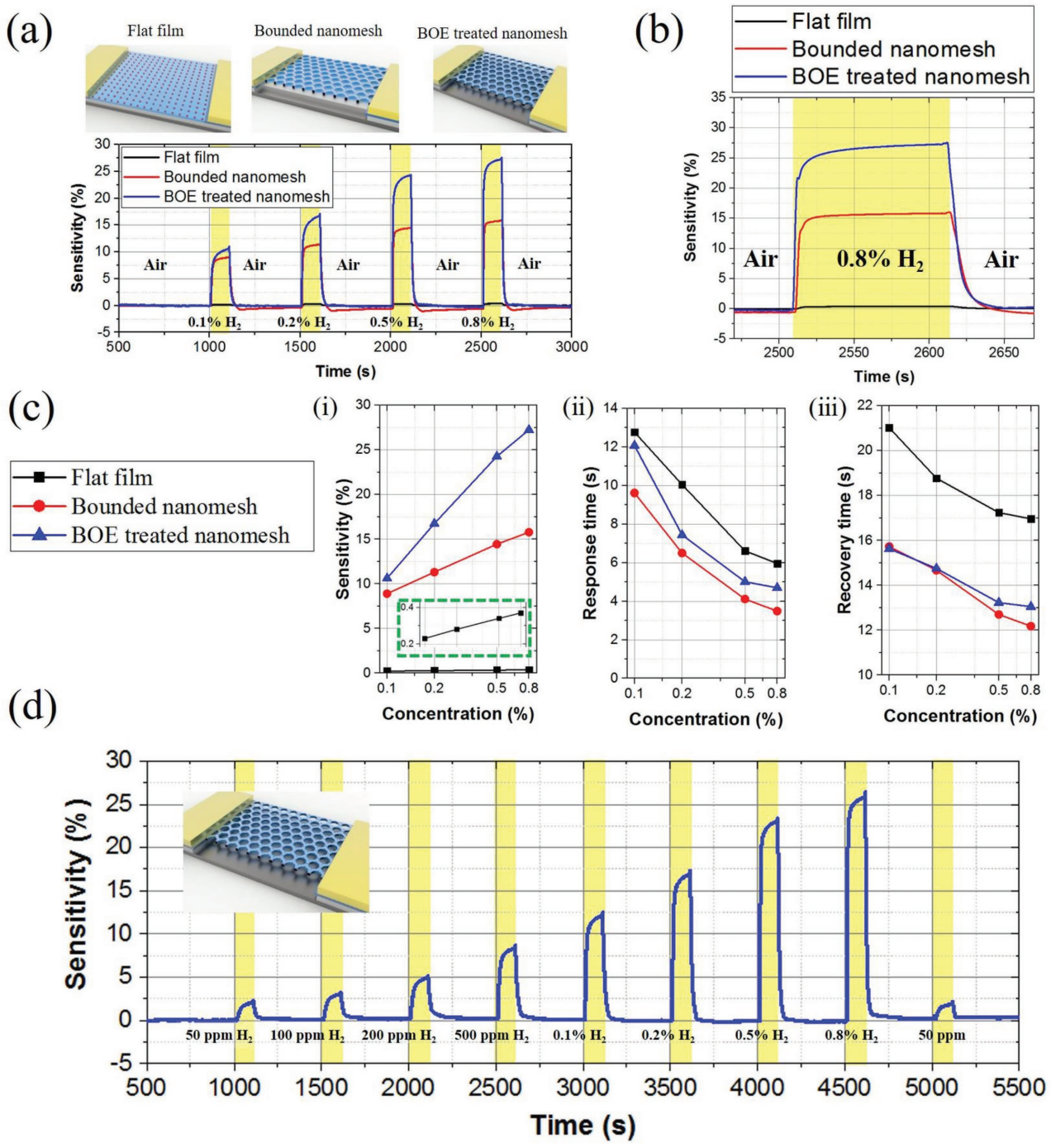

Figure 4. H_2 responses of sensors upon exposure to H_2 at various concentrations: a) real-time sensing signal to 0.1%, 0.2%, 0.5%, and 0.8% H_2 for sensors with a flat film channel, bounded Si nanomesh channel, and BOE treated Si nanomesh channel; b) close-up view of the response to 0.8% H_2; c-i) sensitivity, c-ii) response time, and c-iii) recovery time for three different type sensors to H_2 concentrations of 0.1%, 0.2%, 0.5%, and 0.8%; d) real-time response of the sensor with BOE treated suspended Si nanomesh channel to H_2 with concentrations of 50 ppm – 0.8%.

treatment due to the partial etching of the doped Si by BOE.[42,43] After Pd was decorated on top of the Si surface, an electron depletion layer was formed in the Si channel due to the high work function of the deposited PdNPs, causing an increase in resistance. This effect of the Pd layer as a gate on the Si channel is schematically illustrated in Figure 3b. The numerical simulation in Figure 3c using a semiconductor device simulator (ATLAS in SILVACO Inc.) reveals that the electron concentration changed after Si surface was coated with the Pd layer, with a work function of 5.12 eV (details of the numerical simulation process are provided in Figure S4, Supporting Information).

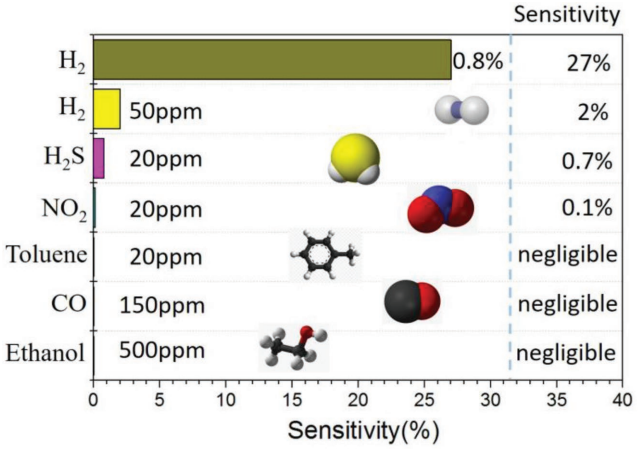

Figure 5. Selective gas sensing performance of the BOE treated Si nanomesh sensor against other interfering gases with corresponding critical concentrations.

To demonstrate the gas sensing properties of the Si nanomesh sensor, a gas sensing test was carried out with different concentrations of H_2 target gas. Based on the requirement from the US Department of Energy, H_2, which has a LFL of 4% in air and an alarm concentration level of 0.4% (10% of the LFL), a safety action should take place at 1% (25% of the LFL).[47] Thus, the range of H_2 concentrations close to these critical values are the most interesting for H_2 safety monitoring applications. In order to avoid serious danger to humans, the H_2 sensor needs to rapidly respond to these critical concentrations. The general sensing mechanism of the Pd-gated-Si H_2 sensor, which has already been explained in the Introduction, is illustrated in Figure S5 in the Supporting Information. To evaluate the effect of Pd loading on the sensor device, Si film structures with and without Pd decoration were tested, and a comparison of their H_2 sensing performance is shown in Figure S6 in the Supporting Information.

To further confirm the effect of each fabrication step on the H_2 sensing performance, devices fabricated with a flat film channel without the nanomesh pattern, a bounded nanomesh structure (when the BOE treatment process shown in Figure 1d is omitted), and a suspended Si nanomesh structure after BOE treatment were compared with respect to their H_2 sensing performance (detailed schematics of the device structures and their corresponding cross-section views are shown in Figure S7, Supporting Information). Their sensing performances are presented in **Figure 4**. Here, the sensitivity is defined as Sensitivity = $100 \times (I - I_0)/I_0$ in which I and I_0 represent the electrical currents in the target gas and in ambient air, respectively. The response time is the elapsed time from the baseline current to 80% of the saturation value and the recovery time is the elapsed time to reach the initial state from 80%. Figure 4a shows the real-time sensing characteristics of the fabricated sensors with H_2 concentrations of 0.1%, 0.2%, 0.5%, and 0.8%.

A close-up view of the response to 0.8% H_2 is illustrated in Figure 4b to clearly visualize the sensitivity, response, and recovery behaviors of the sensors. The values for the sensitivity, response time, and recovery time are compared in Figure 4c(i)–(iii). The dynamic sensor response shows that the sensitivity for 0.8% H_2 gas increases from 0.37% for the flat film device to 16% for the bounded nanomesh device, which is about a 43 times improvement. For the BOE treated nanomesh device, the sensitivity is about 27%, which is more than 73 times higher than the flat Si film device. The enhancement in sensitivity of the sensors from the bounded film to the nanomesh structure is due to the small dimension (minimum feature: ≈80 nm) of the nanomesh structure: the large surface to volume ratio of the nanomesh structure provides more efficient surface modification by PdNPs.[48] As for the improvement after the channel was suspended by BOE etching, it is thought to be caused by the change in surface morphology. It has been revealed that the BOE treatment results in a slight etching of the Si, which generates a rough and porous surface.[42,43] This phenomenon causes an increased surface area for the loading of PdNPs on the Si surface. This is consistent with the AFM analysis of the Si structures obtained before and after BOE treatment, as shown in Figure S3 in the Supporting Information.

For 0.8% of H_2, the 80% response time was 4.7, 3.5, and 6.0 s for the flat Si film, the bounded Si nanomesh and the BOE treated Si nanomesh structure, respectively. The fast response and recovery characteristics originate from the small dimension of the PdNPs on the Si surface.

AFM images of the SOI substrate with and without PdNPs are illustrated in Figure S3 in the Supporting Information. The RMS value of the surface roughness increased from 0.344 nm for the SOI substrate to 0.66 nm after 2 min of

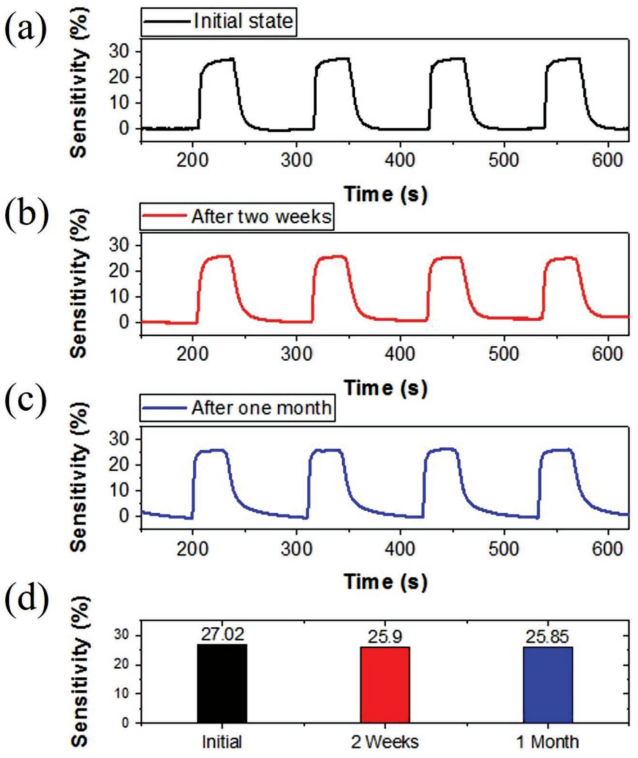

Figure 6. Short-time repeatability and long-time stability of the BOE treated Si nanomesh sensor: a) 0.8% H_2 sensing test response at initial state, b) response after 2 weeks, c) response after 1 month, and d) change in sensitivity along time elapse.

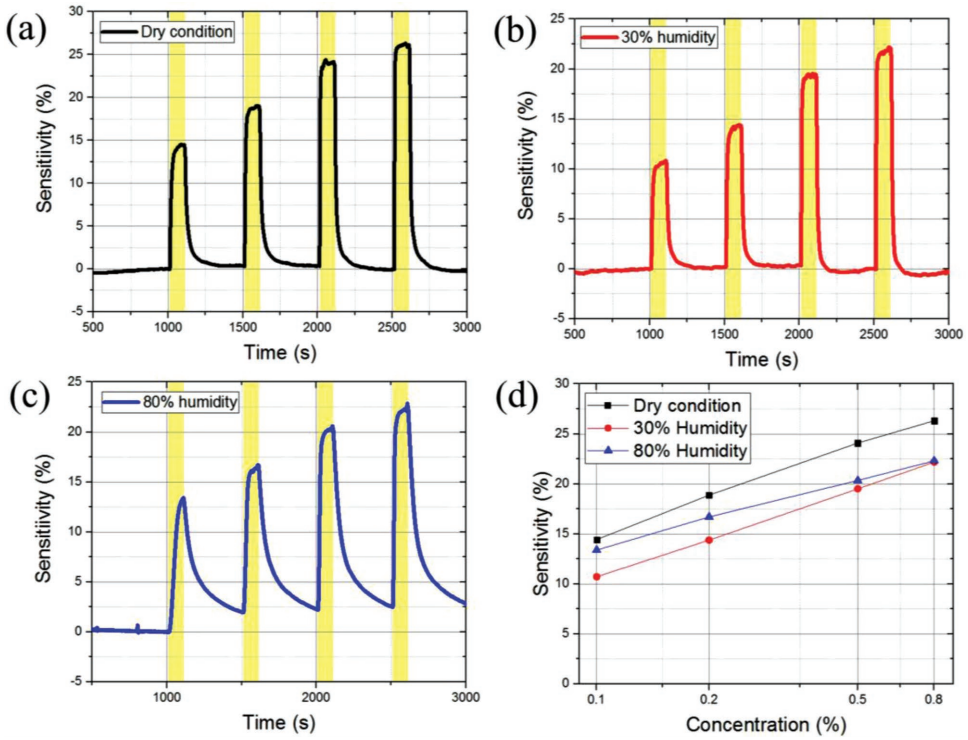

Figure 7. Dynamic H_2 (with concentrations of 0.1%, 0.2%, 0.5%, 0.8%) sensing performance under a) dry condition; b) 30% RH condition; c) 80% RH condition; and d) the sensitivity values under dry, 30% RH, and 80% RH conditions.

BOE treatment, and further increased to 2.069 nm after 1 nm Pd coating via e-beam evaporation. These PdNPs exhibit a larger surface to volume ratio than previously reported Pd nanowire-based H_2 sensors. Faster response and recovery characteristics were observed with small dimension Pd detection elements.[3]

A detection test with H_2 concentrations from 50 ppm to 0.8% was conducted with the BOE treated nanomesh sensor, as shown in Figure 4d. The results show that the sensor has a lower limit of detection (LOD) below 50 ppm, with a clear and distinguishable signal to H_2 concentrations from 50 ppm to 0.8%, with fast response and recovery. In addition, a similar response (from 2.21% to 2.16%) to 50 ppm was observed after exposure to 0.8%, with a nonsignificant memory effect, proving the good reversibility and repeatability of the sensor.

The selectivity of the BOE treated Si nanomesh H_2 sensor to other potentially interfering gases, such as hydrogen sulfide (H_2S), nitrogen dioxide (NO_2), and carbon monoxide (CO), was investigated with the corresponding critical concentration of each gas.[49] The responding sensitivity for these analytes is shown in **Figure 5**. The results reveal that the sensor has a remarkably higher H_2 response in the concentration range from 50 ppm (sensitivity ≈ 2%) to 0.8% (sensitivity ≈ 27%) over other interfering gases at the normal critical concentrations. The sensor shows a sensitivity of 0.76% to 20 ppm H_2S and 0.11% to 20 ppm NO_2, which are within the concentration ranges of lethal or dangerous conditions.[49] Furthermore, the sensor showed negligible sensitivities to toluene, CO, and ethanol. These results confirm the device has excellent H_2 selectivity, which is due to the fact that Si is inert to these gases, and Pd has a good selective response to H_2.

The repeatability and stability of the performance of the BOE treated Si nanomesh sensor was investigated by comparing its response at an initial state, after two weeks, and one month later. The sensor was stored in a clean room environment without any further special conditions. **Figure 6** shows the dynamic responses to our cycles of 0.8% H_2: the sensor showed reversible and consistent responses in each of the repeated test cycles. In addition, the sensors maintained good long-term stability for a one month period. As shown in Figure 6, the sensitivity value exhibited only a slight variation from 27.02% to 25.90% and to 25.85% after 2 weeks and 1 month, respectively.

The effect of humidity on the response to H_2 gas was investigated using a BOE treated Si nanomesh sensor for the H_2 concentrations of 0.1%, 0.2%, 0.5%, and 0.8% in air with three different humidity conditions—dry, 30% relative humidity (RH), and 80% RH. As shown in **Figure 7**, under these humidity conditions, our sensor exhibited sensitivity degradation as the RH increased. The sensor maintained a fast response and recovery speeds under the dry condition and 30% RH. However, at high humidity (80% RH), the response and recovery speed became much slower. In high RH, water vapor condenses on the Pd surface, blocking the ability of the surface to adsorb H_2 molecules, and thus reducing the response speed.[50]

Since Pd-related nanomaterials have been extensively developed as outstanding materials for H_2 detection, a comparison of recently developed Pd nanomaterial-based H_2 sensors is summarized in **Table 1**. PdNPs and Pd nanowires (PdNWs) are popular sensing materials because of their fast response and

Table 1. Comparison of some recently reported (2015–2017) Pd-nanomaterial-based H_2 sensors.

Materials	Fabrication method[a)]	t_{res}/t_{rec}[b)] @ ≈0.1% [H_2]	Response[c)] @ ≈0.1% [H_2]	t_{res}/t_{rec} @ ≈1% [H_2]	Response @ ≈1% [H_2]	Dynamic range[d)]	Selectivity	Humidity effect[e)] (RH range)	Working temp.[f)]	Reference
Pd nanoparticles @ Si nanomesh	Nanosphere lithography	12 s (t_{80})/16 s (t_{20})	10%	5 s (t_{80})/13 s (t_{20})	27%	50 ppm ≈0.8%	H_2S, NO_2, CO, toluene, ethanol	<20% (0% ≈80%)	RT	This work
Pd nanoparticles @ Si nanowire	Deep UV lithography	18 s (t_{80})/12 s (t_{20})	0.8%	nr	nr	0.1–0.5%	CO	<20% (10%–70%)	RT	[3]
Pd-Ni thin layer @ Si nanosheet	Oxidation and etching	nr	nr	30 s (t_{90})/30 s (t_{50})	≈600%	0.3–2%	H_2S, NO_2	nr	RT	[14]
Pt @ Pd nanowire	Bottom-up growth	250 s (t_{90})/15 s (t_{10})	<1%	nr	nr	500 ppm ≈5%	nr	nr	RT	[10]
zeolite imidazole framework (ZIF) @ Pd nanowire	Bottom-up growth	30 s (t_{90})/8 s (t_{10})	0.7%	nr	nr	600 ppm ≈1%	nr	nr	RT	[51]
Pd @ WO_3 nanofiber	Electrospinning	nr	nr	nr	nr	10 ≈ 500 ppm	CH_4, CO, NH_3	> 80% (0–90%)	450 °C	[6]

[a)]Here, the fabrication method involves a main current channel structure like the Si nanomesh in this work; [b)]Abbreviations: t_{res} = response time and t_{rec} = recovery time; for response time, t_{80} means the time necessary for the resistance (or current) to change from R_0 to $R_0 + 0.8\Delta R_{max}$; for recovery time, t_{20} means the time necessary for the resistance (or current) to change from $R_0 + \Delta R_{max}$ to $R_0 + 0.2\Delta R_{max}$, nr = not reported; [c)]Response = $\Delta R_{max}/R_0$ (or $\Delta I_{max}/I_0$); [d)]Dynamic range is the gas concentration measured in the paper, it may not exactly mean the limited working range for the sensors; [e)]Humidity effect is the difference in responses at different humidity conditions; [f)]Abbreviation: RT = room temperature.

recovery ability, enabled by the small dimensional structure. The PdNW-based chem-resistive sensor showed fast response but suffered from low sensitivity and high LOD; however, the response sensitivity was circumscribed by the limited resistance change caused by H_2 adsorption, and thus a small lower LOD could not be achieved.[10,51] The Pd-metal oxide hybrid material-based H_2 sensors, such as Pd-WO_3 nanofibers, can achieve an LOD as small as several ppm, but their high working temperature and humidity interference could restrict their applications.[6]

Our work focused on a Pd-decorated Si structure for the H_2 sensor application, and by using nanosphere lithography and simple BOE treatment method, the fabrication cost was reduced compared with the costs of devices fabricated via conventional high-resolution lithography methods.[3] At the same time, the present work with a Pd-decorated Si nanomesh demonstrated it provides a fast and distinguishable response to H_2 gas over a wide detection range (50 ppm to 0.8%) at room temperature, with excellent selectivity and low interference from humidity. The overall performance is improved, compared with the previous studies.

3. Conclusion

In summary, a high-performance and low-cost H_2 sensor with a PdNPs-decorated Si nanomesh structure was developed using a simple and facile fabrication process via polystyrene nanosphere lithography. The small dimensions of the Si enhanced the Pd-gating effect and thus dramatically improved the sensitivity. Also, the use of nanosphere lithography, avoided the need for an expensive high-resolution lithography process. The BOE treatment roughened the Si surface, resulting in a clear improvement in sensitivity, by increasing the surface to volume ratio. Additionally, the sensor with PdNPs-decorated Si nanomesh channel structure showed excellent selectivity against common interfering gases. Compared with other conventional Si-based H_2 sensors, the Si nanomesh sensors can be fabricated using a low cost process and show better performance. It is expected that our approach will be very useful for the fabrication of low cost, high performance sensors for chemical and biological detection with applications to mobile and wearable devices at the coming era of internet of things.

4. Experimental Section

Sensor Fabrication: P-type SOI wafers were utilized for the sensor fabrication. The thickness of top Si layer and BOX layer were 60 and 400 nm, respectively. Active area was formed via conventional UV-lithography and reactive-ion etching (RIE) for top Si layer (RIE condition: 90 mTorr, O_2/SF_6). The area for metallization was doped by arsenic (As) ion implantation (dose 5×10^{15} cm^{-2}, energy 25 keV), giving an impurity concentration as high as 10^{21} cm^{-3} (n^+-Si). A low doping phosphorus (P) ion implantation (dose 1×10^{14} cm^{-2}, energy 15 keV) was then applied to the entire area, which gave a relatively low doping centration with around 10^{18} cm^{-3} (n^--Si) at the channel area. A 10 nm thick Cr layer was later deposited on top of the n^+-Si area to protect the highly doped region from etching in the later PS-NSL patterning process. Afterward, the PS-NSL process was applied for the nanostructure pattern of the top Si in the n^--Si channel area (see the next Experimental Section). After the pattern transfer of top Si in the n^--Si channel area, Cr layer including the hard mask and the protection layers was removed by chromium wet etchant (Cr-7). The nanomeshed Si channel region was 20 µm in width and 20 µm in length. Metal contacts consisting of Cr/Au (10/200 nm) were deposited by electron beam (e-beam) evaporation. Buffered-oxide-etchant (BOE 6:1) treatment later was employed to the entire area for 2 min. Finally, 1 nm thin Pd layer was deposited on the surface of the channel area by e-beam evaporation, achieving selective response to H_2. Since the deposited thickness is too thin, Pd was aggregated to isolated PdNPs.[3] The electrical properties were measured by Keithley 2423 (DC voltage sweep).

PS-NSL Nanopatterning and Transfer Etching: The SOI wafer was cut into 2 cm × 2 cm chip size before the PS-NSL process, followed by a

30 min acetone bath and 30 min DI water bath under sonication to remove the surface contamination. PS beads with a diameter of 500 nm (from Polysciences, Inc.) were used in the nanosphere lithography. The compact monolayer of PS beads was formed on substrate via multistep spin coating process.[44,45] Oxygen (O_2) plasma was used to control the size of the beads, creating nanogaps between individual beads. A Cr layer was deposited on top of the PS-coated substrate. After the removal of PS beads by DI water bath under mild sonication, a honeycomb-like nanomesh structure consisting of Cr was formed on top of the PS-coated substrate. The Cr structure served as the hard mask in the following RIE process (condition: 90 mTorr, O_2/SF_6) for Si etching to transfer the same pattern to the Si substrate. Since the n^+-Si was covered by a protection layer in advance, only the n^--Si channel area could be patterned.

Gas Detection: The gas sensing performance of the fabricated sensor was tested in a sealed chamber with a probe station inside. A schematic of the gas test setup is shown in Figure S8 in the Supporting Information. The real-time channel current was recorded via a sourcemeter (Keithley 2635B) when target gas with certain concentration was injected into the chamber. The mixture gases of N_2 and O_2 with a volume ratio of 4:1 was used to represent air environment, which represent the basic state of the sensor. The composition and the concentration of the test gas were controlled by adjusting the flow rate of the corresponding mass-flow controllers (MFCs) while the total flow rate was maintained at 500 sccm. The current sourcemeter and MFCs were all controlled by the LabView interface.

Supporting Information

Supporting Information is available from the Wiley Online Library or from the author.

Acknowledgements

This work was supported by the Nano Material Technology Development Program (2015M3A7B7045518) and Grant No. 2017M3D9A1073858 through the National Research Foundation (NRF) of Korea funded by the Ministry of Science, ICT and Future Planning. It is also part of the Project titled "Development of Management Technology for HNS Accident", funded by the Ministry of Oceans and Fisheries, Korea.

Note: The acknowledgements were updated on March 8, 2018 after initial online publication.

Conflict of Interest

The authors declare no conflict of interest.

Keywords

hydrogen sensors, nanosphere lithography, palladium nanoparticles, Si surface texturing, silicon nanowires

Received: October 23, 2017
Published online: January 25, 2018

[1] T. Hubert, L. Boon-Brett, G. Black, U. Banach, *Sens. Actuators, B* **2011**, *157*, 329.
[2] S. K. Arya, S. Krishnan, H. Silva, S. Jean, S. Bhansali, *Analyst* **2012**, *137*, 2743.
[3] J. H. Ahn, J. H. Yun, D. I. Moon, Y. K. Choi, I. Park, *Nanotechnology* **2015**, *25*, 095501.
[4] M. A. Lim, D. H. Kim, C. O. Park, Y. W. Lee, S. W. Han, Z. Y. Li, R. S. Williams, I. Park, *ACS Nano* **2012**, *6*, 598.
[5] R. Ramachandran, R. K. Menon, *Int. J. Hydrogen Energy* **1998**, *23*, 593.
[6] S. J. Choi, S. Chattopadhyay, J. J. Kim, S. J. Kim, H. L. Tuller, G. C. Rutledge, I. D. Kim, *Nanoscale* **2016**, *8*, 9159.
[7] T. Samerjai, N. Tamaekong, C. Liewhiran, A. Wisitsoraat, A. Tuantranont, S. Phanichphant, *Sens. Actuators, B* **2011**, *157*, 508.
[8] F. A. Lewis, *The Palladium Hydrogen System*, Academic, New York **1967**.
[9] F. Favier, E. C. Walter, M. P. Zach, T. Benter, R. M. Penner, *Science* **2001**, *293*, 2227.
[10] X. W. Li, Y. Liu, J. C. Hemminger, R. M. Penner, *ACS Nano* **2015**, *9*, 3215.
[11] J. H. Ahn, J. H. Yun, Y. K. Choi, I. Park, *Appl. Phys. Lett.* **2014**, *104*, 013508.
[12] S. Mubeen, T. Zhang, B. Yoo, M. A. Deshusses, N. V. Myung, *J. Phys. Chem. C* **2007**, *111*, 6321.
[13] K. I. Lundstrom, M. S. Shivaraman, C. M. Svensson, *J. Appl. Phys.* **1975**, *46*, 3876.
[14] H. M. Fahad, H. Shiraki, M. Amani, C. Zhang, V. S. Hebbar, W. Gao, H. Ota, M. Hettick, D. Kiriya, Y. Chen, Y. Chueh, A. Javey, *Sci. Adv.* **2017**, *3*, e1602557.
[15] C. K. Jeong, H. M. Jin, J. H. Ahn, T. J. Park, H. G. Yoo, M. Koo, Y. K. Choi, S. O. Kim, K. J. Lee, *Small* **2014**, *10*, 337.
[16] J. M. Halpern, B. Wang, H. Haick, *ACS Appl. Mater. Interfaces* **2015**, *7*, 11315.
[17] Y. Cui, Q. Wei, H. Park, C. M. Lieber, *Science* **2001**, *293*, 1289.
[18] F. Patolsky, C. M. Lieber, *Mater. Today* **2005**, *8*, 20.
[19] X. Chen, C. K. Y. Wong, C. A. Yuan, G. Q. Zhang, *Sens. Actuators, B* **2013**, *177*, 17.
[20] N. Shehada, J. C. Cancilla, J. S. Torrecilla, E. S. pariente, G. Bronstrup, S. Christiansen, D. W. Johnson, M. Leja, M. P. A. Davies, O. Liran, N. Peled, H. Haick, *ACS Nano* **2016**, *10*, 7047.
[21] J. Yun, C. Y. Jin, J. H. Ahn, S. Jeon, I. Park, *Nanoscale* **2013**, *5*, 6851.
[22] Y. Paska, T. Stelzner, O. Assad, U. Tisch, S. Christiansen, H. Haick, *ACS Nano* **2012**, *6*, 335.
[23] Y. Cui, Z. H. Zhong, D. Wang, W. U. Wang, C. M. Lieber, *Nano Lett.* **2003**, *3*, 149.
[24] F. Patolsky, G. Zheng, C. M. Lieber, *Nat. Protoc.* **2006**, *1*, 1711.
[25] M. C. Mcalpine, H. Ahmad, D. Wang, J. R. Heath, *Nature* **2007**, *6*, 379.
[26] I. Park, Z. Li, A. P. Pisano, R. S. Williams, *Nanotechnology* **2010**, *21*, 015501.
[27] J. W. Han, T. Rim, C. K. Baek, M. Meyyappan, *ACS Appl. Mater. Interfaces* **2015**, *7*, 21263.
[28] W. Lu, C. M. Lieber, *Nat. Mater.* **2007**, *6*, 841.
[29] R. G. Hobbs, N. Petkov, J. D. Holmes, *Chem. Mater.* **2012**, *24*, 1975.
[30] C. Vieu, F. Carcenac, A. Pepin, Y. Chen, M. Mejias, A. Lebib, L. Manin-Ferlazzo, L. Couraud, H. Launois, *Appl. Surf. Sci.* **2000**, *164*, 111.
[31] V. R. Manfrinato, A. Stein, L. Zhang, C. Nam, K. G. Yager, E. A. Stach, C. T. Black, *Nano Lett.* **2017**, *8*, 4562.
[32] P. Colson, C. Jemrost, R. Cloots, *J. Nanomater.* **2013**, *8*, 948510.
[33] C. L. Haynes, R. P. Van Duyne, *J. Phys. Chem. B* **2001**, *105*, 5599.
[34] D. Ji, T. Li, H. Fuchs, *Adv. Electron. Mater.* **2016**, *3*, 1600348.
[35] S. Su, L. Lin, Z. Li, J. Feng, Z. Zhang, *Nanoscale Res. Lett.* **2013**, *8*, 405.
[36] J. R. Oh, J. H. Moon, H. K. Park, J. H. Park, H. Chung, J. Jeong, W. Kim, Y. R. Do, *J. Mater. Chem.* **2010**, *20*, 5025.
[37] L. Li, Y. Fang, C. Xu, Y. Zhao, K. Wu, C. Limburg, P. Jiang, K. J. Ziegler, *ACS Appl. Mater. Interfaces* **2017**, *9*, 7368.
[38] M. Kang, M. Losego, E. Sachet, J. P. Maria, S. Franzen, *ACS Photonics* **2016**, *3*, 1993.
[39] K. Seo, M. Wober, P. Steinvurzel, E. Schonbrun, Y. Dan, T. Ellenbogen, K. B. Crozier, *Nano Lett.* **2011**, *11*, 1851.

[40] H. J. In, C. R. Rield, P. E. Pehrsson, *Nanotechnology* **2011**, *22*, 355501.
[41] Y. Qin, Y. Wang, Y. Liu, X. Zhang, *Nanotechnology* **2016**, *27*, 465502.
[42] S. M. Hu, D. R. Kerr, *J. Electrochem. Soc.* **1967**, *114*, 414.
[43] G. Willeke, K. Kellermann, *Semicond. Sci. Technol.* **1996**, *11*, 415.
[44] J. Chen, P. Dong, D. Di, C. Wang, H. Wang, J. Wang, X. Wu, *Appl. Surf. Sci.* **2013**, *270*, 6.
[45] A. Chandramohan, N. V. Sibirev, V. G. Dubrovskii, M. C. Petty, A. J. Gallant, D. A. Zeze, *Sci. Rep.* **2017**, *7*, 40888.
[46] J. Nah, S. B. Kumar, H. Fang, Y. Chen, E. Plis, Y. Chueh, S. Krishna, J. Guo, A. Javey, *J. Phys. Chem. C* **2012**, *116*, 9750.
[47] Summary and Findings from the NREL/DOE Hydrogen Sensor Workshop, http://www.nrel.gov/docs/fy12osti/55645.pdf (accessed: August 2017).
[48] C. Guo, L. Luo, G. Yuan, X. Yang, R. Zhang, W. Zhang, S. Lee, *Angew. Chem., Int. Ed.* **2009**, *48*, 9896.
[49] Immediately Dangerous To Life or Health (IDLH) Values – Table of IDLH Values, https://www.cdc.gov/niosh/idlh/intridl4.html (accessed: August 2017).
[50] Z. Zhan, M. A. Carpenter, H. Xia, D. Welch, *Sens. Actuators, B* **2006**, *113*, 532.
[51] W. Koo, S. Qiao, A. F. Ogata, G. Jha, J. Jang, V. T. Chen, I. Kim, R. M. Penner, *ACS Nano* **2017**, *11*, 9276.

